RSC Advances

ROYAL SOCIETY OF CHEMISTRY

www.rsc.org/advances

Experimental and theoretical studies on the corrosion inhibition of mild steel by some Sulphonamides in Aqueous HCl

Lutendo C. Murulana[a,b,c], Mwadham M. Kabanda [b,c], Eno E. Ebenso[b,c,*]

[a]Department of Chemistry, School of Mineral and Physical Sciences, University of Limpopo (Turfloop Campus), Private Bag X1106, Sovenga 0727, South Africa.
[b] Material Science Innovation & Modelling (MaSIM) Research Focus Area, Faculty of Agriculture, Science and Technology, North-West University (Mafikeng Campus), Private Bag X2046, Mmabatho 2735, South Africa.
[c] Department of Chemistry, North-West University (Mafikeng Campus), Private Bag X2046, Mmabatho 2735, South Africa.

*Corresponding Author; E-mail: Eno.Ebenso@nwu.ac.za; Tel: +27 183892050/2051; Fax: +27183892052

Abstract

Corrosion inhibition studies of mild steel in aqueous HCl by some sulphonamides namely Sulphamethazine (SMT), Sulphachloropyridazine (SCP), Sulphabenzamide (SBZ) and Sulphaquinoxaline (SQX) has been investigated using experimental techniques (such as weight loss, Potentiodynamic Polarization (PDP), Electrochemical Impedance Spectroscopy (EIS), Fourier Transform Infrared Spectroscopy (FTIR) and Scanning Electron Microscopy (SEM)) and theoretical method (using the Density Functional Theory (DFT). All the compounds effectively inhibited the corrosion process by becoming adsorbed on the metal surface following the Langmuir adsorption isotherm model. The electrochemical results showed that these inhibitors are mixed-type. The theoretical studies were undertaken to provide mechanistic insight into the roles of the different substituents on the corrosion inhibition and adsorption behaviour of the studied compounds. The calculated quantum chemical parameters include the highest occupied molecular orbital (HOMO), the energy of the HOMO, dipole moment and partial atomic charges, etc. The calculated molecular properties were compared across the structures of the four compounds in order to identify trends related to their reactivity and their corrosion inhibition ability. The results also show that the ability of the sulphonamides to inhibit metal corrosion is strongly dependent on the electron donating ability of the substituent group and that the preferred site for interaction with the metal surface, in all the sulphonamides, is the SO_2 group.

Keywords Electrochemical techniques, Mild steel, FTIR, reactivity parameters, DFT, selectivity indices, SEM.

1. Introduction

The use of organic compounds to prevent or reduce the corrosion of metal surfaces is widely recognised mainly because these substances are economically viable in comparison to other approaches that are utilised in the prevention of corrosion. However, some of the organic corrosion inhibitors are considered to be less environment-friendly because after their utilisation, they do not leave the environment. Research is increasingly oriented towards the search for organic compounds, and other compounds such as ionic liquids, that have eco-friendly effects on the environment [1-6]. The adsorption of the inhibitor molecule on the metal surface depends strongly on its physico-chemical properties such as functional groups present, electronic density at the donor atom and geometry of the molecular structure [7–11].

Sulphonamides are organic compounds which exhibit excellent characteristics of good corrosion inhibitors including the presence of nitrogen, oxygen and sulphur heteroatoms that have lone pair of electrons, the presence of multiple bonds and the presence of aromatic rings that are electron rich [11, 12]. Moreover, sulphonamides can be considered environmentally friendly because of their frequent use as medicinal drugs. Despite their valuable utilisation in pharmaceutical industries, there have been limited studies on the utilisation of sulphonamides as corrosion inhibitors [12]. In the current study four sulphonamides namely, Sulphamethazine (SMT), Sulphachloropyridazine (SCP), Sulphabenzamide (SBZ) and Sulphaquinoxaline (SQX) have been selected for the study to identify their structural and electronic properties that make them good corrosion inhibitors. The molecular structures and the numbering of the atoms for the selected structures are shown in Figure 1. The objective of the current work is to utilize experimental techniques in acidic medium such as potentiodynamic polarization, electrochemical impedance, weight loss, Fourier Transform Infrared Spectroscopy and Scanning Electron Microscopy to gain insight into the adsorption mechanism of the selected sulphonamides at the mild steel surfaces. The compounds utilised in this study were tested in the HCl media, rather than in other media such as ordinary water or saline water, because acidic media is more corrosive than both neutral and saline water environments. It is therefore assumed that if the compounds tested in this work can withstand the corrosiveness of HCl acid, they will also be suitable corrosion inhibitors in less acidic media. The study considers different temperatures and different concentrations of the selected inhibitor. Quantum chemical calculations are also utilised to investigate the molecular geometric parameters and electronic parameters necessary for understanding the reactivity of the different inhibitors.

2. Experimental Procedure

2.1 Mild steel specimens

All experimental procedures involving mild steel were executed using mild steel specimens of composition (wt %): (P = 0.02), (Mn = 0.37), (S = 0.03), (Mo = 0.01), (Ni = 0.039), (C = 0.21) and (Fe = 99.32). These specimens were meticulously prepared prior to all experimental procedures. They were abraded utilizing various grades of emery papers, washed with doubly distilled water followed by acetone and consequently air-dried overnight before their storage in desiccators until such time when they were utilized for all experimental procedures.

2.2 Solutions

All of the working solutions were prepared as reported elsewhere [13]. Aggressive solution of 1.0 M HCl was carefully prepared by diluting Analytical grade 32% Hydrochloric acid from Merck Chemicals through addition of appropriate amounts of doubly distilled water. A stock solution of 10.0 x 10^{-5} M corrosion inhibitors was carefully prepared through the addition of appropriate amount of doubly distilled water. To ensure complete dissolution of the sulphonamides compounds, a ratio of 1:100 of ethanol and doubly distilled water was utilized. From the stock solution, a series of concentrations as indicated in the results section were prepared.

2.3 Electrochemical Techniques

All electrochemical measurements were performed using a Metrohm Autolab Potentiostat/Galvanostat (PGSTAT302N) which employed a three-electrode cell, namely a platinum counter electrode (CE), saturated calomel with Ag/AgCl reference electrode (RE) and mild steel working electrode (WE). Prior to all electrochemical measurements, a 30 min period was allowed as a period of stabilization to establish a steady state open circuit potential. Potentiodynamic polarization curves were measured at the potential range of -250 to +250 mV (SCE) and scan rate of 1 $mV.s^{-1}$. Electrochemical Impedance curves were measured using a frequency response analyser (FRA) connected to the Potentiostat/Galvanostat at the frequency range of 100 kHz to 0.00001 kHz under potentiodynamic conditions with amplitude of 10 mV peak-to-peak, using AC signal at E_{corr}. The mild steel specimens utilized had a 1 cm^2 surface area exposed to the corrosive solution.All these measurements were done at atmospheric conditions without any stirring.

2.4 Weight loss measurements

Most studies indicate that weight loss method is the most preferred method for the corrosion studies mainly because of its simplicity, accurateness, preciseness and reliability [13, 14-16]. Weight loss measurements were carried out as previously reported in our works [13]. Mild steel specimens were totally immersed in corrosive solutions of 1.0 M HCl in the absence and presence of various concentrations of all studied corrosion inhibitors at 30-50 °C for a total immersion time of 15 h. Parameters such as percent inhibition efficiency (Eq. 1) and corrosion rates (Eq. 2) were calculated using the equations below:

$$\%\, IE_{WL} = \left(1 - \frac{w_1}{w_0}\right) \times 100 \qquad (1)$$

Where w_0 is the weight loss of mild steel in the absence of corrosion inhibitors and w_1 is the weight loss of mild steel in the presence of corrosion inhibitors.

$$\rho = \frac{\Delta w}{St} \qquad (2)$$

Where Δw is the average weight loss of mild steel in (g), S is the surface area of mild steel in (cm^2) and t is the total immersion time in (s).

2.5 Fourier Transform Infrared Spectrometer (FTIR)

Adsorption films that were formed during the corrosion of mild steel in 1.0 M HCl in the absence and presence of all studied corrosion inhibitors at 30 °C were carefully scratched off the mild steel surfaces with a sharp scissors and the resultant powder was investigated using Nicolet iS5 Fourier Transform Infrared Spectrometer.

2.6 Surface Analysis

Mild steel specimens with a surface area of 1 cm^2 were treated with 1.0 M HCl in the absence and presence of all studied corrosion inhibitors at 30 °C. Their surface morphology and Energy Dispersive Spectroscopy (EDS) analysis were performed using JOEL JSM-7500F Field Emission Scanning Electron Microscope.

2.7 Computational methods

All geometry optimizations and quantum chemical calculations were performed using density functional theory (DFT) utilising the Becke's Three Parameter and the Lee-Yang-Parr correlation functional theory (B3LYP) [17]. The 6-31+G(d,p) basis set was also selected for the study. Density functional theory (DFT) has found wide applicability in the analysis of the characteristics of the inhibitor/metal surface mechanisms and in the description of the structural nature of the inhibitor on the corrosion process [18, 19]. Moreover, there is a good agreement between experimental results and the quantum chemical parameters computed using DFT [19]. Some of the chemical parameters calculated include chemical hardness, chemical softness, electron affinity and polarization potential. Chemical hardness (η) measures the resistance of an atom to a charge transfer [20], and it is estimated by using the equation:

$$\eta \cong -\tfrac{1}{2} (E_{HOMO} - E_{LUMO}) \quad (3)$$

Chemical softness (σ) describes the capacity of an atom or group of atoms to receive electrons [20] and is estimated by using the equation:

$$\sigma = 1/\eta \cong -2/(E_{HOMO} - E_{LUMO}) \quad (4)$$

Electron affinity (A) is related to E_{LUMO} through the equation:

$$A \cong - E_{LUMO} \quad (5)$$

Ionization potential (I) is related to the energy of the E_{HOMO} through the equation:

$$I \cong - E_{HOMO} \quad (6)$$

All calculations were done by using the Gaussian09 program [21]. Schematic structures were drawn using the ChemOffice package in the UltraChem 2010 version while optimized structures were drawn using the gaussView5 program.

3. Results and discussion

3.1 Potentiodynamic polarization (PDP)

Mild steel corrosion comprises a simultaneous anodic dissolution of mild steel and the cathodic reduction of hydrogen ions [22]. Potentiodynamic polarization measurements were carried out in order to fully understand this process. To facilitate this objective, the current-potential curves for mild steel in hydrochloric acid solutions were obtained in the absence and presence of various concentrations of the four sulphonamides at 30 °C, and the curves are shown in Figure 2. The curves in this figure show both anodic and cathodic half-reactions of the mild steel corrosion in hydrochloric acid. It is also observed that both half-reactions are affected by the introduction of all four inhibitors. From these curves, a successful extrapolation of their linear Tafel segments produced some valuable potentiodynamic parameters such as corrosion current density (i_{corr}), corrosion potential (E_{corr}), anodic Tafel slope (b_a) and cathodicTafel slope (b_c). These parameters are recorded in Table 1. The potentiodynamic polarization inhibition efficiency ($\%IE_{PDP}$) was then calculated from equation (7) [22]:

$$\%IE_{PDP} = \left(\frac{i^{0}{}_{corr} - i^{i}{}_{corr}}{i^{0}{}_{corr}} \right) \times 100 \qquad (7)$$

where i^{0}_{corr} and i^{i}_{corr} are the corrosion current densities in the absence and presence of inhibitor molecules, respectively.

Both Figure 2 and Table 1 show that the introduction of all four inhibitors significantly reduced the corrosion current densities for both anodic and cathodic half-reactions, which suggests that both anodic dissolution of mild steel and cathodic reduction of the hydrogen ions were inhibited. The trend in the values of E_{corr} shows consistency and a minimal change, with a change within the range of 20-40 mV. This type of behaviour from the E_{corr} values is attributed to mixed-type inhibitors [23, 24]. The values of anodic and cathodic Tafel slopes for inhibited processes show some variations when compared to those of their blank counterparts. This indicates that both anodic and cathodic half-reactions are affected by the presence of the inhibitor molecules. The inhibition efficiency values obtained from PDP increase with the increase in the concentration of the inhibitors utilized in the study. It is reasonable to infer that the inhibition process could be caused by the formation of the adsorption film resulting from the interaction between mild steel surface and the sulphonamide inhibitor molecules. The results from PDP study also correlates well with the ones obtained from weight loss measurements.

3.2 Electrochemical impedance spectroscopy (EIS)

Further information regarding the characteristics and kinetics of mild steel corrosion in acidic solutions and the inhibition by sulphonamides compounds was obtained using electrochemical impedance spectroscopy. The main advantage of electrochemical impedance spectroscopy is to follow the corrosion behaviour of the metal with time. Nyquist plots, represented by the imperfect semicircles shown in Figure 3, shows the impedance spectra for mild steel corrosion in 1.0 M HCl solution in the absence and presence of various concentrations of the four inhibitor compounds utilized at 30 °C while their corresponding Bode plots are shown in Figure 4. These imperfect semicircles increase their diameter with the increase in inhibitor concentrations, and this imperfection is an indication of the formation of the adsorption film on the surface of mild steel and a charge transfer process which governs the corrosion of mild steel in acidic solutions [25].

Observation of Nyquist plots in Figure 3 shows both depressed capacitive and inductive loops at high-frequency (HF) and low-frequency (LF), respectively. Previous studies have shown that the low-frequency inductive loop is attributed to bulk relaxation process due to the adsorption of charged species onto the charged metal surfaces while the high-frequency capacitive loop is attributed to the charge transfer and double layer capacitance (C_{dl}) [26, 27].

The impedance nature of the corrosion reactions was explained utilizing a simple electrical equivalent circuit comprising the resistor (R_s), resistance of charge transfer (R_{ct}) and a double layer capacitance, as reported elsewhere [28-30]. In order to obtain a more accurate and representative fit, the double layer capacitance was replaced by the constant phase element (CPE) as shown in Figure 5. The CPE is defined by the expression:

$$Z_{CPE} = \frac{1}{Y_0 (j\omega)^n} \tag{8}$$

where Y_0 is the CPE constant, ω is the angular frequency, j is the imaginary number and n is the phase shift (exponent) which is related to the degree of surface inhomogeneity [31]. Depending on the value of n, CPE can represent resistance (n=0, Y_0 = R), capacitance (n=1, Y_0 = C), inductance (n =−1, $Y_0 = L$) or Warburg impedance (n = 0.5, $Y_0 = W$).

The electrochemical impedance parameters such as R_s, R_{ct}, CPE, n and $\%IE_{EIS}$ were calculated following the equation below.

$$\%IE_{EIS} = \left(1 - \frac{R_{ct}^0}{R_{ct}}\right) \times 100 \tag{9}$$

where R^0_{ct} and R_{ct} are the resistances of charge transfer in the absence and presence of inhibitors, respectively.

The results of the calculations of these parameters are reported in Table 2. The values of R_{ct} provides details on the magnitude of the electron transfer over the mild steel surface and are inversely proportional to the inhibition efficiency [25]. A close examination of the values in Table 2 shows that as the concentration of all four inhibitors is increased, R_{ct} also increases while CPE decreases. This behaviour is a direct result of the increased surface coverage on mild steel by the inhibitor molecules as a result of their increased concentration. Furthermore, the reduction in CPE indicates the decrease in dielectric constant and an enhancement of the thickness of the electrical double layer. This is a consequence of the adsorption of sulphonamides compounds on the mild steel/ hydrochloric acid interface which brings about the prevention of further corrosion of mild steel [33, 34]. The values of 'n' are constant and close to unity which signifies that the interface is of a capacitive nature. The results from EIS correspond very well with those obtained from PDP and weight loss measurements except in less frequent cases where some discrepancies were noticed.

3.3 Adsorption film analysis

The FT-IR technique is useful in studying the adsorption film resulting during the adsorption process [35]. The FT-IR spectra of the studied corrosion inhibitors as well as the adsorption films formed on the mild steel surface using different corrosion inhibitors are shown in Figure 6. Sulphonamides possess several functional groups that

have high electron density. This implies that the adsorption film between vacant *d*-orbitals of the metal and the sulphonamides is most likely to take place within these functional groups. Table 3 shows the characteristic absorption bands corresponding to the main electron source groups within the studied compounds and compares them with those that are obtained from the adsorption film of the inhibited process. The characteristic absorption bands within the wavenumber range of 1190-1130 cm^{-1} corresponds to the C-N stretch for secondary amine [33], 3490-3430 cm^{-1} and 3360-3310 cm^{-1} to heterocyclic amine N-H stretch and aliphatic secondary amine N-H stretch, respectively [34, 36], 1650-1590 cm^{-1} to NH_2 primary amine N-H bend [33], 1350-1325 cm^{-1} to O=S=O [32] and 1600, 1500 cm^{-1} to aromatic, conjugated C=C [33, 34]. The presence of bands at 3371.95 cm^{-1}, 1638.98 cm^{-1}, 1607.95 cm^{-1}, 1136.85 cm^{-1} and 667.21 cm^{-1} corresponding to N-H stretch, NH_2 group, aromatic conjugated C=C, C-N stretch and γ-Fe_2O_3, respectively for SQX signifies the formation of SQX-Fe^{2+} complex. Similar discussions can be used regarding SMT, SBZ and SCP as reported in Table 3 and shown in Figure 6. Nevertheless, a meticulous examination of all FT-IR spectra of inhibitor-Fe^{2+} complex in the absorption range between 1700-500 cm^{-1} shows that most of the characteristic absorption bands have disappeared. The disappearance of O=S=O, which is one of the possible electron donor, is more pronounced with respect to all four inhibitors. Another interesting observation is made with regard to SMT which shows the disappearance of a band corresponding to N-H, which is another possible electron donor. Therefore, the O=S=O functional group is the most preferred site for interaction with the mild steel surface. The lone pair of electrons on the O atoms in this functional group could donate electrons to the vacant or partially filled d orbitals of the Fe metal atoms and thereby result in the formation of a chemical bond and in the eventual protection of the metal surface. The N-H functional group from SMT also shows reactivity to some extent. The last row in Table 3 shows the characteristic absorption bands in the region of 450-700 cm^{-1} for all inhibitors. Literature indicates that these bands correspond to the passivating iron oxide layers (γ-Fe_2O_3) [36]. These layers are formed during the corrosion of mild steel in acidic medium. Studies have shown that passivating layers of iron oxide can also aid protection of mild steel from further destruction by the aggressive ions in acidic solutions [37, 38].

3.4 Surface analysis

SEM micrographs and their corresponding EDS spectra for various mild steel specimens were studied in order to gain more insight into the adsorption process taking place during the corrosion process. The results are shown in Figures 7 and 8, respectively. From Figure 7a, it is evident that the surfaces of mild steel prior immersion in hydrochloric acid solutions exhibit smooth nature with minor damages that might be due to the abrasion with various emery papers. Nevertheless, these surfaces exhibit more rough nature after their immersion in hydrochloric acid solutions as shown in Figure 7b. A consideration of the corresponding EDS spectra in Figures 8a and 8b show the absence and presence of aggressive Cl^- ions, respectively which are responsible for the destruction of the smooth surfaces of mild steel [35, 39-41]. A comparison of SEM micrographs of mild steel in the presence of all four corrosion inhibitors utilized in this study with those of the uninhibited surfaces shows that the availability of inhibitor compounds prevents the surfaces of mild steel from corrosion. This is evident from the smooth surfaces shown in Figures 7c-f. The corresponding EDS spectra for images 7c-f are shown in Figures 8c-f. From these spectra it is easy to see that the absence of Cl^- ions is pronounced. It can be inferred that the sulphonamides utilized exhibit better inhibition efficiency through the formation of the adsorption film on the mild steel surface. Similar observations were reported by Tang *et al* [42] and Thiraviyam *et al* [43], who

concluded that protective adsorption films reduces corrosion rate and enhances inhibition efficiency due to the fact that they reduce the contact between mild steel surfaces and the acidic solutions.

3.5 Corrosion rate and inhibition efficiency

The variation of percentage inhibition efficiency from the weight loss measurements ($\%IE_{WL}$) with inhibitor concentration is shown in Figure 9. The trend of the $\%IE_{WL}$ versus inhibitor concentration is almost similar for all four inhibitors studied at 30-50 °C. All four inhibitors exhibit the highest $\%IE_{WL}$ at their highest concentration of 5.0 x 10^{-5} M. The main reason behind this is the fact that at 5.0 x 10^{-5} M there is a greater availability of inhibitor molecules than at 1.0 x 10^{-5} M. The presence of more inhibitor molecules leads to a greater tendency of adsorption of inhibitor molecules on the surface of the metal, thus higher $\%IE_{WL}$.

Table 4 shows the corrosion rates and $\%IE_{WL}$ for mild steel corrosion in 1.0 M HCl in the absence and presence of various concentrations of the inhibitors at 30-50 °C. The results of the study suggests that the corrosion rate increases with an increase in temperature of the surrounding environment but decreases with an increase in inhibitor concentration for all four inhibitors. The corrosion rate for mild steel in 1.0 M HCl in the absence of the corrosion inhibitors was found to increase from 0.0023 $g.cm^{-2}.h^{-1}$ to 0.0039 $g.cm^{-2}.h^{-1}$ and then 0.0075 $g.cm^{-2}.h^{-1}$ at 30 °C, 40 °C and 50 °C, respectively. However, in the presence of corrosion inhibitors, these values are greatly reduced. This observation is due to the fact that at higher temperatures molecules within the system have more energy and thus move with higher average kinetic speeds leading to higher corrosion rate. Nevertheless, as the inhibitor concentration is increased, the presence of inhibitor molecules within the system is increased and thus improves the adsorption of the inhibitor molecules on the surface of the metal thereby lowering the corrosion rate.

3.6 Kinetic parameters: Effect of temperature

An increase in temperature of the surrounding environment leads to an increase in mild steel corrosion rate [13]. There are numerous parameters that are directly or indirectly related to this behaviour, amongst them is the activation energy. The activation energy (E_a) of mild steel corrosion is the minimum amount of energy that mild steel components (mainly Fe), acidic medium components, oxygen and moisture would require in order to produce the corrosion products, such as rust. High mild steel dissolutions are associated with low E_a values while low dissolutions are associated with higher values. Arrhenius equation is very useful in terms of evaluating the effect of temperature on the adsorption tendencies and determination of activation parameters for mild steel corrosion [13, 44]. Equation 10 shows the type of Arrhenius equation used to calculate E_a for mild steel corrosion [44, 45]:

$$\log C_R = \log A - \frac{E_a}{2.303RT} \qquad (10)$$

where C_R is the corrosion rate in $g.cm^{-2}.h^{-1}$, A is the Arrhenius pre-exponential factor, R is the gas constant and T is the absolute temperature. The values of E_a are recorded in Table 5 and were calculated from the slopes and intercepts of the Arrhenius plots shown in Figure 10. The E_a values increase with the increase in the concentrations of inhibitor molecules. It is also noticed that E_a corresponding to the uninhibited mild steel

corrosion is always less than that of the inhibited process. This implies that mild steel dissolution in 1.0 M HCl is reduced through the formation of inhibitor-Fe complex. Figure 11 shows the variations of activation energy with the concentration of the utilized corrosion inhibitors.

Further information regarding the effect of temperature on the inhibition efficiency was obtained from activation parameters such as enthalpy of activation (ΔH*) and entropy of activation (ΔS*). The corrosion rate and temperature is related to these parameters through transition-state equation of the form [44, 45]:

$$\log \frac{C_R}{T} = \left[\log\left(\frac{R}{hN}\right) + \left(\frac{\Delta S^*}{2.303\,R}\right)\right] - \frac{\Delta H^*}{2.303\,RT} \qquad (11)$$

where h is the Plank`s constant ($6.63\times10^{-34}$Js) and N is the Avogadro`s number (6.023×10^{23} mol^{-1}). A plot of $\log(C_R/T)$ against (1/T), shown in Figure 12, enabled the calculation of ΔH* and ΔS* from the slope and intercept of the regression line. These values are also recorded in Table 5.

The adsorption process between mild steel surface and inhibitor molecules can be classified as either exothermic or endothermic. In general terms, exothermic process gives off heat and may suggest either chemisorption or physisorption whereas endothermic process entirely suggests chemisorption [44, 46]. Chemisorption involves the sharing of electron pairs with the vacant *d*-orbitals of Fe in mild steel while physisorption involves the electrostatic interactions between charged mild steel surfaces and charged inhibitor molecules [46]. Positive values of the enthalpy of activation in the present study signifies the fact that mild steel dissolution process is of endothermic nature, comparison of the values of enthalpy of activation for the uninhibited process to that of inhibited shows that the inhibited process has higher values. This observation supports the fact that there is an adsorption process that took place between the inhibitor molecules and surfaces of mild steel. Studies show that numerical values of enthalpy of activation ranging up to 41.86 $kJ.mol^{-1}$ are associated with physisorption type of adsorption whereas those around 100 $kJ.mol^{-1}$ or higher are associated chemisorption [47]. Table 5 shows that the values of enthalpy of activation are slightly less than those of their respective activation energies and are above 41.86 $kJ.mol^{-1}$ yet slightly less than 100 $kJ.mol^{-1}$. This kind of behaviour may be attributed to a mixed-type of adsorption of mild steel adsorption and the type of adsorption correlates very well with the correlation predicted by the electrochemical measurements.

Entropy of activation provides some further insight into the mild steel adsorption process. This parameter assists with information regarding the extent of disorder of the adsorption/desorption process between mild steel and inhibitor compounds. The values of entropy of activation, reported in Table 5, shows that as the concentration of the inhibitor molecules is increased, the entropy is also increased. Similar trend in entropy of activation values against inhibitor concentrations was reported by Singh and Quraishi [46], who attributed this behaviour to the fact that there is an increase in disorder during the adsorption process on going from reactants to activated complex [46].

3.7 Thermodynamic parameters: Adsorption Isotherms

Corrosion inhibitors normally protect mild steel through adsorbing onto its surface. This process may adopt a chemisorption, physisorption or mixed-type mode. A typical adsorption phenomenon between the corrosion

inhibitor and metal surface involves the replacement of water molecule at a corroding interface according to the pattern represented in equation 12 [48]:

$$SFA_{(sol)} + nH_2O_{(ads)} \Leftrightarrow SFA_{(ads)} + nH_2O_{(sol)} \quad (12)$$

where SFA is the sulfanoamide corrosion inhibitor and n is the size ratio of the number of molecules replaced by adsorbed molecules. The efficiency of the corrosion inhibitor shows the ability to be adsorbed on the metal surface by displacing the water molecule from the interface which is attacked by corrosion. In order for us to completely understand the adsorption mechanism, it is important to assume a quasi-equilibrium adsorption through application of a suitable adsorption isotherm. This assumption is considered reasonable due to the fact that the adsorption phenomenon on the corroding mild steel surface never achieves a complete equilibrium but instead achieves an adsorption steady-state [48]. Various adsorption isotherms were fitted in the current investigation, including Langmuir, Freundlich, Flory-Huggins, BET, Temkin and Frumkin. Nevertheless, the maximum values of regression coefficients (r^2) from the linear relationship showed that Langmuir adsorption isotherm was the most appropriate isotherm. The numerical values of (r^2) and slopes are recorded in Table 6 and 7. A direct relationship between the surface coverage of the sulphanoamides corrosion inhibitors on the mild steel surface and the concentration of these inhibitors is best given by the Langmuir adsorption isotherm according to the following equation [49-51].

$$\frac{\theta}{1-\theta} = K_{ads} C_{inh} \quad (13)$$

where K_{ads} is the equilibrium constant for the adsorption of inhibitor molecules on the mild steel surface, C_{inh} is the molar concentration of inhibitor molecules and θ is the degree of surface coverage of inhibitor molecules on the mild steel surface. Rearrangement of this equation produces a much simpler relationship of the form:

$$\frac{C_{inh}}{\theta} = \frac{1}{K_{ads}} + C_{inh} \quad (14)$$

Langmuir plots are shown in Figure 13 (as obtained from the weight loss methods) and Figure 14 (as obtained from the electrochemical methods) and they enabled the calculation of the values of adsorption equilibrium constants. The significance of these values lies in the fact that they can be interpreted to provide information regarding the strength between the adsorbate molecules and the adsorbate surfaces; an efficient adsorption process that leads to better inhibition efficiency is often obtained when the adsorption equilibrium constants have large values. From values of adsorption equilibrium constants, standard free energy of adsorption can be calculated as:

$$\Delta G^{\circ}_{ads} = -RT \ln(55.5 K_{ads}) \quad (15)$$

where ΔG° is the standard free energy of adsorption and the value 55.5 represents the molar concentration of water in solution. Studies indicates that values of ΔG°_{ads} varying between -40 $kJ.mol^{-1}$ and above are symbolic of the sharing or transfer of an electron from the adsorbate molecules to the substrate surfaces resulting into a coordinate type of bond (chemisorption) while those around -20 $kJ.mol^{-1}$ and lower are symbolic of an

electrostatic interaction between the charged adsorbate and charged surfaces of the substrate (physisorption) [51, 52]. The values of ΔG°_{ads} reported in Table 6 shows a negative nature which is an indication of spontaneity of the adsorption process and the stability of the adsorbed film on the surface of mild steel [4]. The trend in these values is utilized to further explain the nature of adsorption between mild steel and corrosion inhibitors. In cases where ΔG°_{ads} increases with increase in temperature, an exothermic adsorption is predominant whereas in cases where ΔG°_{ads} decreases with increase in temperature indicates the occurrence of an endothermic adsorption [43]. The values of ΔG°_{ads} are increasing with increase in temperature, thus the adsorption between mild steel surface and sulfonamides inhibitors is of an exothermic nature which signifies either chemisorption or physisorption. This inhibitor behaviour correlates very well with the one predicted by the electrochemical measurements.

3.8 Quantum chemical Calculation methods

To be able to explain the inhibition performance of the studied sulphonamide derivatives, we investigated the molecular reactivity and selectivity descriptors for these molecules. The schematic representations and the optimized geometries of the studied sulphonamides are shown in Figure 1. All the quantum chemical data that are used for comparison with experimental results relate only to the lowest-energy conformer of each of these compounds. The reactivity of the sulphonamides was investigated by analysing the frontier molecular orbitals. According to the frontier molecular orbital theory, chemical reactivity is strongly determined by the interaction of the highest occupied molecular orbital (HOMO) and the lowest unoccupied molecular orbital (LUMO) of the interacting species [52]. The HOMO densities are also shown in Figure 1. In SMT, SCP and SBZ structures, the HOMO is of π bonding character and is strongly localised in the aminobenzene region, and on the sp^2 O atoms of the SO_2 group; in SQX the HOMO is delocalised throughout the whole molecule. This result suggests that an electrophilic attach would probably occur in the aminobenzene group and the SO_2 group.

Other quantum chemical parameters were computed to have more insight in the reactivity and selectivity of the studied compounds. The frontier molecular orbital energies (i.e., E_{HOMO} and E_{LUMO}) provide information on the reactivity of chemical species. The E_{HOMO} is often associated with the electron donating ability of a molecule [54-56] and a higher E_{HOMO} energy value indicates higher tendency of the molecule to donate electron(s) to the appropriate acceptor molecule with low energy and empty/partially filled molecular orbital. This implies that molecules with high values of E_{HOMO} have a greater tendency to adsorb and would probably have higher metal corrosion inhibition efficiency than other compounds. The results reported in Table 8 show that E_{HOMO} for SMT is the highest and this implies that, among the studied compounds, it has the highest tendency to donate electrons towards the metal surface.

Molecules with large value of ΔEare highly stable (i.e., they have low reactivity to chemical species) while molecules with small values of ΔE have a high reactivity. A molecule with a small value of ΔE is easily polarized and can therefore be easily adsorbed on the metal surface, resulting in appreciably good inhibition efficiency. The data reported in Table 8 show that SMT and SQX have the lowest and the highest ΔE value respectively. The trend in the ΔE values across structures, therefore, does not correlate with the trend in the experimental inhibition efficiency across structures.

The dipole moment (μ) is another index that is often used for the prediction of the direction of a corrosion inhibition process. It is the measure of polarity in a bond and is related to the distribution of electrons in a molecule [56]. Inhibitors with high dipole moment tend to form strong dipole-dipole interactions with the metal,

resulting in strong adsorption on the surface of the metal and therefore leading to greater inhibition efficiency [58]. However, a survey of literature shows that in most cases, experimental inhibition efficiencies do not always correlate with dipole moments [59]. The results reported in Table 8 shows that SMT has the highest dipole moment and SQX has the smallest dipole moment.

The local selectivity of an inhibitor can be analyzed by using condensed Fukui functions that provide information about which atoms in a molecule have a higher tendency to either loose or accept an electron or pair of electrons. The nucleophilic and electrophilic Fukui functions can be calculated using the finite difference approximation as follows [59].

$$f^{+} = q_{(N+1)} - q_N \quad (16)$$

$$f^{-} = q_N - q_{(N-1)} \quad (17)$$

where $q_{(N+1)}$, q and $q_{(N-1)}$ are the charges of the atoms on the systems with N+1, N and N–1 electrons respectively. The preferred site for nucleophilic attack is the atom or region in the molecule where the value of f^{+} is the highest while the site for electrophilic attack is the atom/region in the molecule where the value of f^{-} is the highest. The isosurface figure for the Fukui f^{-} function is shown in Figure 1. The results indicate that the electrophilic site for attack is the amino benzene group, the SO_2 group, which is in agreement with the HOMO analysis.

3.9 The binding strength of the Fe atom on the different sites of sulphonamides

The previous study only identifies the sites on which the metal ion is likely to interact with the sulphonamides. However, the identification of the reactivity and selectivity parameters does not provide information on the site on the sulphonamide with the strongest binding with the metal atom/surface. To identify the site with the strongest interaction with the metal ion, the metal ion was arranged in the vicinity of the different electron rich centre (i.e., the aminobenzene and the O atoms of the SO_2 group) and the resulting input was optimised. Since for all the compounds the common electron rich region is the aminobenzene and the O atoms of the SO_2 group, it was considered relevant that only the SMT compound be utilised in the study of identifying the region with the highest tendency to bind the metal atom. The interaction energy between the inhibitor and the metal was then estimated as the difference between the energy of the complex ($E_{Fe\text{-}X}$) and the sum of the energy of the isolated inhibitor and isolated Fe atom ($E_X + E_{Fe}$) resulting in the equation;

$$E_{interation} = E_{Fe\text{-}X} - (E_X + E_{Fe}) \quad (18)$$

The binding energy (kcal/mol) is the negative of the interaction energy. The complexes of Fe atom with the SMT are shown in Figure 15. The results show that the preferred site for interaction with the metal surface is the O atom of the SO_2 group and the least preferred site is the benzene ring of the aminobenzene group. This result is in agreement with our FTIR results reported earlier, which showed that only the SO_2 functional group is completely consumed during the corrosion process. The disappearance of the SO_2 corresponds to the formation of the complex between the O atom the Fe atom. The result also means that the lone pair of electrons on the O

atoms has the greatest tendency to interact with the metal atom/ surface than both the π electrons of the benzene ring and the lone pair of electrons of the N atom on the amino group.

The charge on the Fe ion in the complex with sulphonamide molecule may provide an indication for the type of reaction between the inhibitor and the metal surface. In the isolated state the Fe atom and each of the sulphonamide molecules have a charge of 0 *e*. The charge of the Fe atom after complexation has been found to be -1.759*e*, which indicates that in the interaction between the sulphonamides and the Fe surface, the Fe atom is reduced through the gain of electrons from the sulphonamides. Therefore, we infer that sulphonamide molecules have the potential to reduce the Fe atom.

4. Conclusions

Four sulphonamides have been investigated as corrosion inhibitors for mild steel in aq. HCl. The following conclusions can be drawn from the results obtained namely:

- The correlation of the results obtained from weight loss, potentiodynamic polarization and electrochemical impedance spectroscopy is very good and satisfactory.
- Potentiodynamic polarization measurements showed that the sulphonamides are mixed-type inhibitors for mild steel surface corrosion in acid solution.
- Electrochemical impedance spectroscopy showed that these inhibitors protect the surfaces of mild steel through the adsorption at the mild steel/ hydrochloric acid interface and hence the inhibition efficiency improved with inhibitor concentration.
- Langmuir adsorption isotherm model described the adsorption of the sulphonamides used in the study.
- Molecular quantum chemical parameters of the selected sulfonamides were investigated using DFT/B3LYP method. The outcome of the study suggests that the trends in the quantum chemical parameters, across inhibitors, correlates well with the trends in the experimental inhibition efficiency of the inhibitors.
- The analysis of the inhibitor-Fe interactions indicates that the preferred site for the interaction is the SO_2 group, what is also in conformity with the experimental data.
- Sulphonamides corrosion inhibitors exhibit good inhibition efficiency and can be applied in epoxy or paint formulations to improve the longevity of the metals.

Acknowledgements

LCM acknowledges Dr Abolanle S. Adekunle (North West University, Mafikeng Campus) and Ms Charity Maepa (Council for Scientific and Industrial Research, CSIR, South Africa) for their technical assistance in performing the electrochemical measurements and SEM surface analysis, respectively. EEE acknowledges support from the National Research Foundation (NRF) of South Africa for incentive funding.

References

1. B. Hmamou, R. Salghi, A. Zarrouk, M. R. Aouad, O. Benali, H. Zarrok, M. Messali, B. Hammouti, E.E. Ebenso, M. Bouachrine, M. M kabanda, *Ind. Eng. Chem. Res*., 2013, **52**, 14315– 14327.
2. M. M. Kabanda, I. B. Obot, E. E. Ebenso, *Int. J. Electrochem. Sci*., 2013, **8**, 10839 –10850.
3. I.B. Obot, E. E. Ebenso, M. M. Kabanda, *J. Environ. Chem. Eng*., 2013, **1**,431– 439.
4. L. C. Murulana, A. K. Singh, S. K. Shukla, M. M. Kabanda, E. E. Ebenso, *Ind. Eng. Chem. Res*., 2012, **51**, 13282–13299.

5. E. E. Ebenso, M. M. Kabanda, L. C. Murulana, A. K. Singh, S. K. Shukla, Ind. Eng. Chem. Res., 2012, **51**, 12940–12958.
6. M. M. Kabanda, S. K. Shukla, A. K. Singh, L. C. Murulana, E. E. Ebenso, *Int. J. Electrochem. Sci*., 2012, **7**, 8813–8831.
7. M. M. Kabanda, Eno E. Ebenso, *Int. J. Electrochem. Sci*., 2012, **7**, 8713–8733.
8. M. M. Kabanda, L. C. Murulana, E. E. Ebenso, *Int. J. Electrochem. Sci*., 2012, **7**, 7179–7205.
9. M. M Kabanda, L. C. Murulana, M. Ozcan, F. Karadag, I. Dehri, I.B. Obot, E. E. Ebenso. *Int. J. Electrochem. Sci*., 2012, **7**, 5035–5056.
10. S. K. Shukla, A. K. Singh, L. C. Murulana, M. M. Kabanda, E. E. Ebenso, *Int. J. Electrochem. Sci*., 2012, **7**, 5057–5068.
11. T. Arslan, F. Kandemirli, E. E. Ebenso, I. Love, H. Alemu , *Corros. Sci*. 2009, **51**, 35– 47.
12. E. E. Ebenso, T. Arslan, F. Kandemirli, I. Love, C. Öğretil, M. Saracoğlu, S. A. Umoren, *Int. J. Quantum. Chem*., 2010, **110**, 2614–2636.
13. K.M. Manamela, L.C. Murulana, M.M. Kabanda, E.E. Ebenso, *Int. J. Electrochem. Sci*., 2014, **9**, 3029–3046.
14. H. Ashassi-Sorkhabi, M. Es`haghi, *Mater. Chem. Phys*., 2009, **114**, 267-271.
15. I. Belfilali, A. Chetouani, B. Hammouti, S. Louhibi, A. Aouniti, S.S. Al-Deyab, *Res. Chem. Intermed*., 2014, **40**, 1069–1088.
16. N.O. Obi-Egbedi, I.B. Obot, *Arab. J. Chem*., 2012, **5**, 121–133.
17. A.D. Becke, *J. Chem. Phys*., 1993, **98**, 5648 – 5652.
18. J.E. Del Bene, M.J.T. Jordan, *J. Mol. Struct (Theochem)*., 2001, **573**, 11– 23.
19. E. E. Ebenso, T. Arslan, F. Kandemirli, N. Caner, I. Love, *Int. J. Quantum. Chem*., 2010, **110**, 1003–1018.
20. R.G. Parr, R.G. Pearson, *J. Am. Chem. Soc*., 1983, **105**, 7512– 7516.
21. M. J. Frisch, G. W. Trucks, H. B. Schlegel, G. E. Scuseria, M. A. Robb, J. R. Cheeseman, G. Scalmani, V. Barone, B. Mennucci, G. A. Petersson, H. Nakatsuji, M. Caricato, X. Li, H. P. Hratchian, A. F. Izmaylov, J. Bloino, G. Zheng, J. L. Sonnenberg, M. Hada, M. Ehara, K. Toyota, R. Fukuda, J. Hasegawa, M. Ishida, T. Nakajima, Y. Honda, O. Kitao, H. Nakai, T. Vreven, J. A. Montgomery, Jr., J. E. Peralta, F. Ogliaro, M. Bearpark, J. J. Heyd, E. Brothers, K. N. Kudin, V. N. Staroverov, R. Kobayashi, J. Normand, K. Raghavachari, A. Rendell, J. C. Burant, S. S. Iyengar, J. Tomasi, M. Cossi, N. Rega, J. M. Millam, M. Klene, J. E. Knox, J. B. Cross, V. Bakken, C. Adamo, J. Jaramillo, R. Gomperts, R. E. Stratmann, O. Yazyev, A. J. Austin, R. Cammi, C. Pomelli, J. W. Ochterski, R. L. Martin, K. Morokuma, V. G. Zakrzewski, G. A. Voth, P. Salvador, J. J. Dannenberg, S. Dapprich, A. D. Daniels, O. Farkas, J. B. Foresman, J. V. Ortiz, J. Cioslowski, and D. J. Fox, Gaussian, Inc., Wallingford CT, Gaussian 09, Revision *C.01* (2009).
22. M.A. Abu-Dalo, N.A.F. Al-Rawashde, A. Ababneh, *Desalination*., 2013, **313**, 105-114.
23. A.K. Singh, M.A. Quraishi, *J. Appl. Electrochem*., 2011, **41**, 7–18.
24. S.K. Shukla, M.A. Quraishi, *Corros. Sci*., 2009, **51**, 1007–1011.
25. K.S. Jacob, G. Parameswaran, *Corros. Sci*., 2010, **52**, 224–228.
26. H.H. Hassan, E. Abdelghani, M.A. Amin, *Electrochim. Acta*., 2007, **52**, 6359 – 6366.
27. H.H. Hassan, *Electrochim. Acta*., 2007, **53**, 1722–1730.
28. M. El Azhar, B. Mernari, M. Traisnel, F. Bentiss, M. Lagrenee, *Corros. Sci*., 2001, **43**, 2229– 2238.
29. A. Yurt, A. Balaban, S.U. Kandermir, G. Bereket, B. Erk, *Mater. Chem. Phys*., 2004, **85**, 420– 426.
30. D.B. Hmamou, R. Salghi, A. Zarrouk, H. Zarrok, S.S. Al-Deyab, O. Benali, B. Hammouti, *Int. J. Electrochem. Sci*., 2012, **7**, 8988–9003.
31. D.K. Yadav, M.A. Quraishi, B. Maiti, *Corros. Sci*., 2012, **55**, 254– 266.
32. M. Yadav, D. Behera, S. Kumar, R. Sinha, *Ind. Eng. Chem. Res*., 2013, **52**, 6318– 6328.
33. S.A. Umoren, M.M. Solomon, U.M. Eduok, I.B. Obot, A.U. Israel, *J. Env. Chem. Eng*., 2014, **2**, 1048–1060.
34. J. Coates, in: R.A. Meyers (Ed.), Encyclopaedia of Analytical Chemistry, John Wiley and Sons Ltd, Chichester, 2000, pp. 10815– 10837.
35. G. Gunasekaran, L.R. Chauhan, *Electrochim. Acta*., 2004, **49**, 4387– 4395.
36. M.A. Abu-Dalo, A.A. Othman, N.A.F. Al-Rawashde, *Int. J. Electrochem. Sci*., 2012, **7**, 9303–9324.
37. L.R. Chauhan, G. Gunasekaran, *Corros. Sci*., 2007, **49**, 1143– 1161.
38. W.K. Lu, R.L. Elsenbaumer, B. Wessling, *Synthetic.Met*., 1995, **71**, 2163– 2166.
39. P.B. Raja, M.G. Sethuraman, *Mater. Lett*., 2008, **62**, 1602– 1604.
40. A.M. Abdel-Gaber, B.A. Abd-El-Nabey, M. Saadawy, *Corros. Sci*., 2009, **51**, 1038– 1042.
41. W. Li, Q. He, S. Zhang, C. Pei, B. Hou, *J. Appl. Electrochem*., 2011, **38**, 289– 295.
42. Y. Tang, F. Zhang, S. Hu, Z. Cao, Z. Wu, W. Jing, *Corros. Sci*., 2013, **74**, 271– 282.
43. P. Thiraviyam, K. Kannan, *Arab. J. Sci. Eng*., 2013, **38**, 1757– 1767.

44. A. Ostovari, S.M. Hoseinieh, M. Peikari, S.R. Shadizadeh, S.J. Hashemi, *Corros. Sci*., 2009, **51**, 1935– 1949.
45. A.K. Singh, P. Singh, *J. Ind. Eng. Chem*., 2014, http://dx.doi.org/10.1016/j.jiec.2014.03.018.
46. A.K. Singh, M.A. Quraishi, *Corros. Sci*., 2009, **51**, 2752– 2760.
47. N.O. Eddy, E.E. Ebenso, U.J. Ibok, *J. Appl. Electrochem*., 2010, **40**, 445– 456.
48. I.O. Arukalam, I.C. Madufo, O.O. Ogbobe, E.E. Oguzie, *Int. J. Appl. Sci. Eng. Res*., 2014, **3**, 241– 256.
49. M. Abouchane, M. El Bakri, R. Touir, A. Rochdi, O. Elkhattabi, M.E. Touhami, L. Forssal, B.Mernari, *Res. Chem. Intermed*., 2013, doi: 10.1007/s11164-013-1319-5
50. F.S. de Souza, R.S. Goncalves, A. Spinelli, *J. Braz. Chem. Soc*., 2014, **25**, 81– 90.
51. A. El Bribri, M. Tabyaoui, B. Tabyaoui, H. El Attari, F. Bentiss, *Mater. Chem. Phys*., 2013, **141**, 240– 247.
52. I. Belfilali, A. Chetouani, B. Hammouti, S. Louhibi, A. Anouniti, S.S. Al-Deyab, *Res. Chem. Intermed*., 2014, **40**, 1069– 1088.
53. N.O. Obi-Egbedi, I.B. Obot, M.I. El-Khaiary, S.A. Umoren, E.E. Ebenso, *Int. J. Electrochem. Sci*., 2011, **6**, 5649– 5675.
54. N.O. Obi-Egbedi, I.B. Obot, M.I. El-Khaiary, *J. Mol. Struct*., 2011, **1002**, 86– 96.
55. H. Ashassi-Sorkhabi, B. Shaabani, D. Seifzadeh, *Electrochim. Acta*., 2005, **50**, 3446– 3452.
56. I.B. Obot, N.O. Obi-Egbedi*, Curr. Appl. Phys*., 2011, **11**, 382– 392.
57. I.B. Obot, N.O. Obi-Egbedi, *Mater. Chem. Phys*., 2010, **122**, 325– 228.
58. B.D. Mert, M.E. Mert, M.E. Kardas, G. Yazici, *Corros. Sci*., 2011, **53**, 4265– 4272.
59. G. Gece, *Corros. Sci*., 2008, **50**, 2981– 2992.
60. A.K. Chandra, M.T. Nguyen, *Int. J. Mol. Sci*., 2002, **3**, 310– 323.

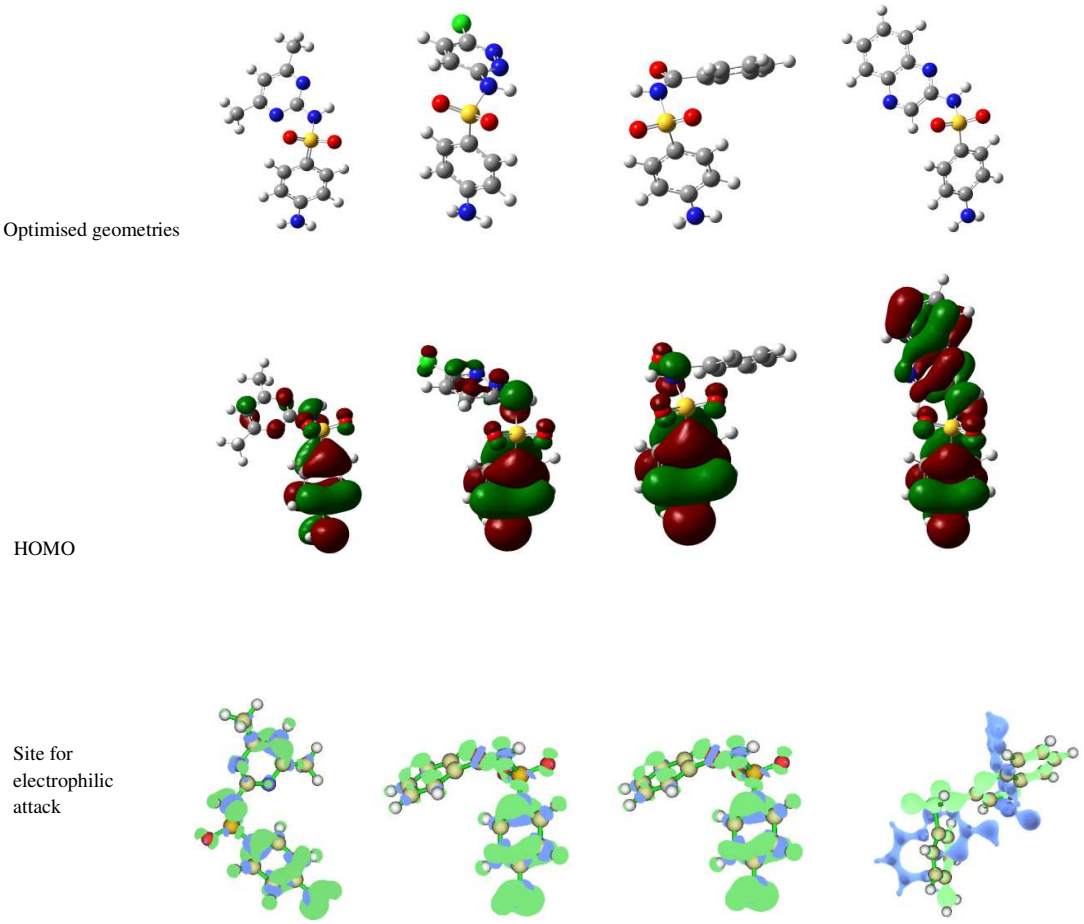

Figure 1. Optimised structure, highest occupied molecular orbital (HOMO) and the site for electrophilic attack (as shown by the Fukui f^- function) for the studied compounds.

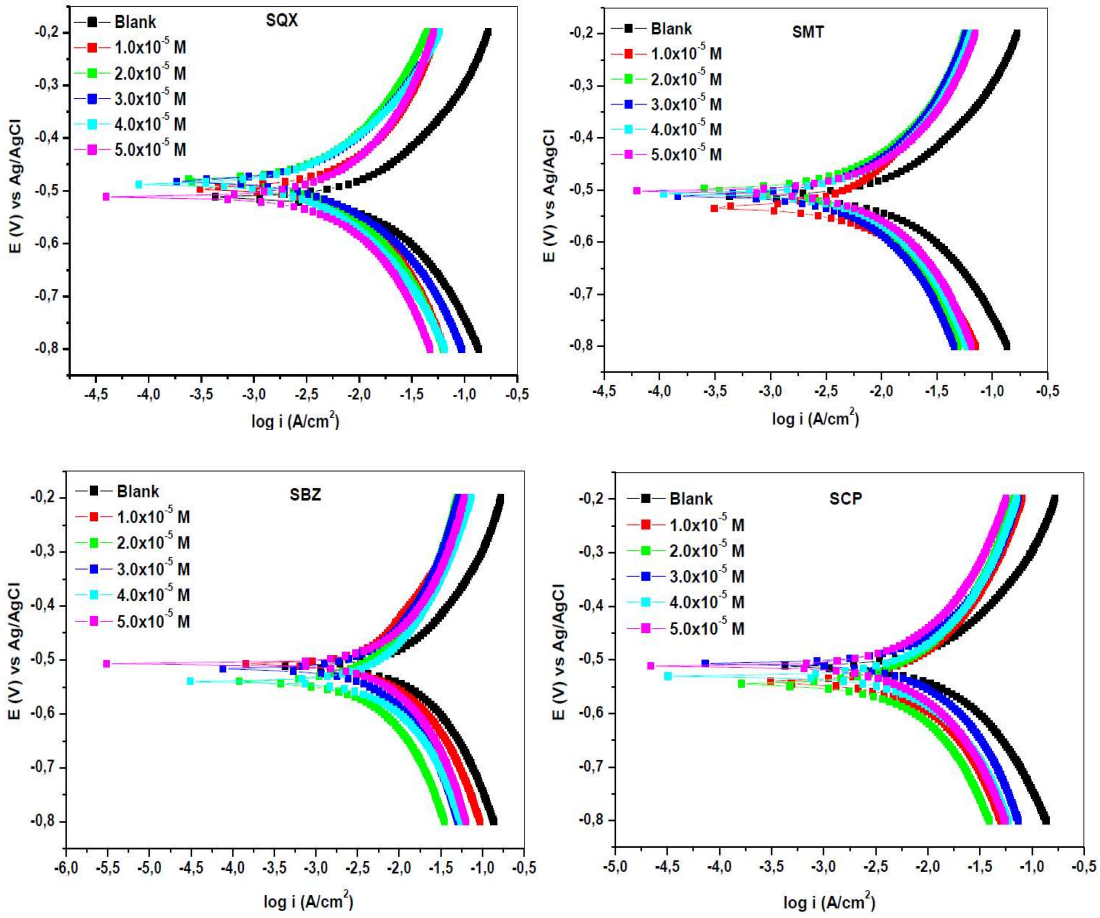

Figure 2. Potentiodynamic polarization curve for mild steel in 1 M HCl in the absence and presence of different concentrations of inhibitor compounds.

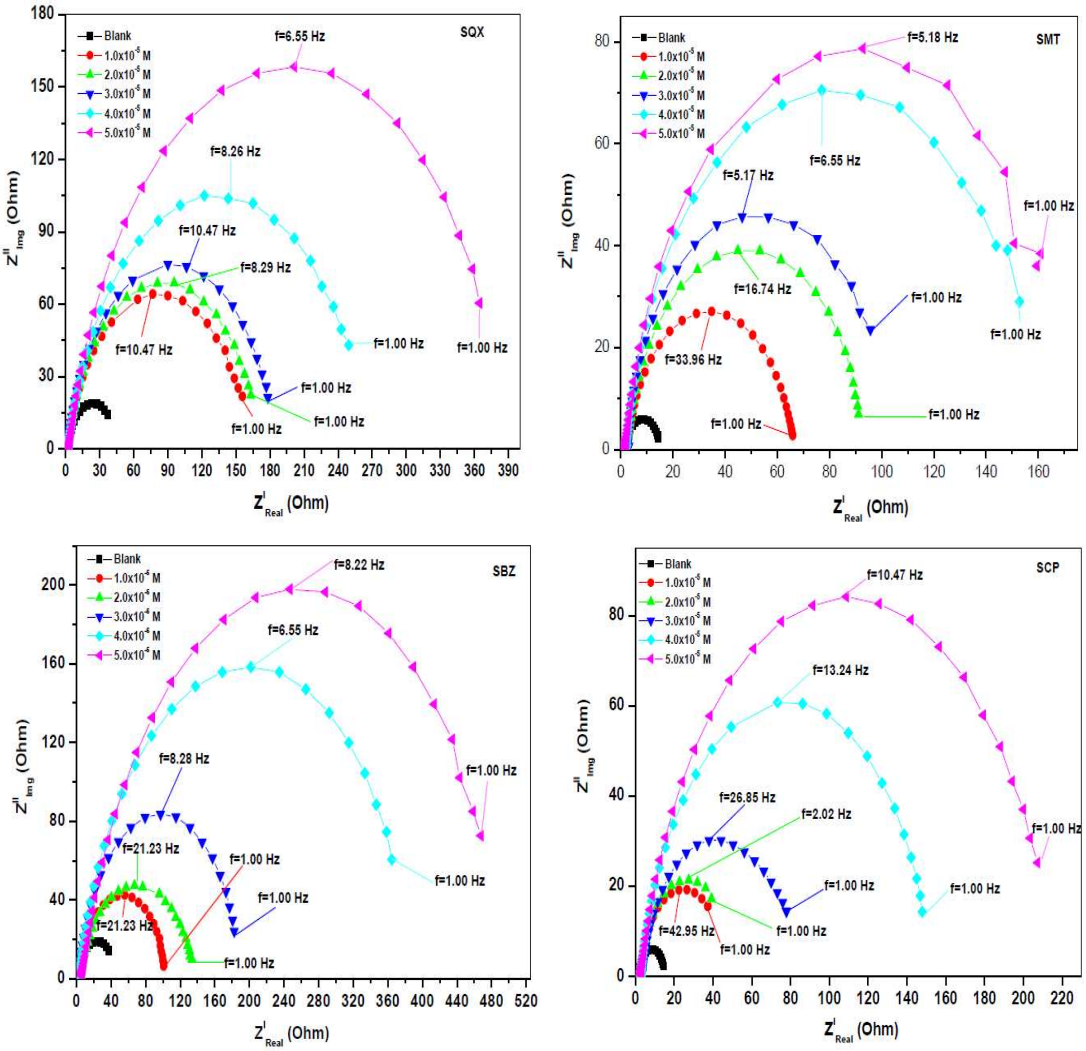

Figure 3. Nyquist plot of mild steel in 1 M HCl in the absence and presence of different concentrations of of inhibitor compounds.

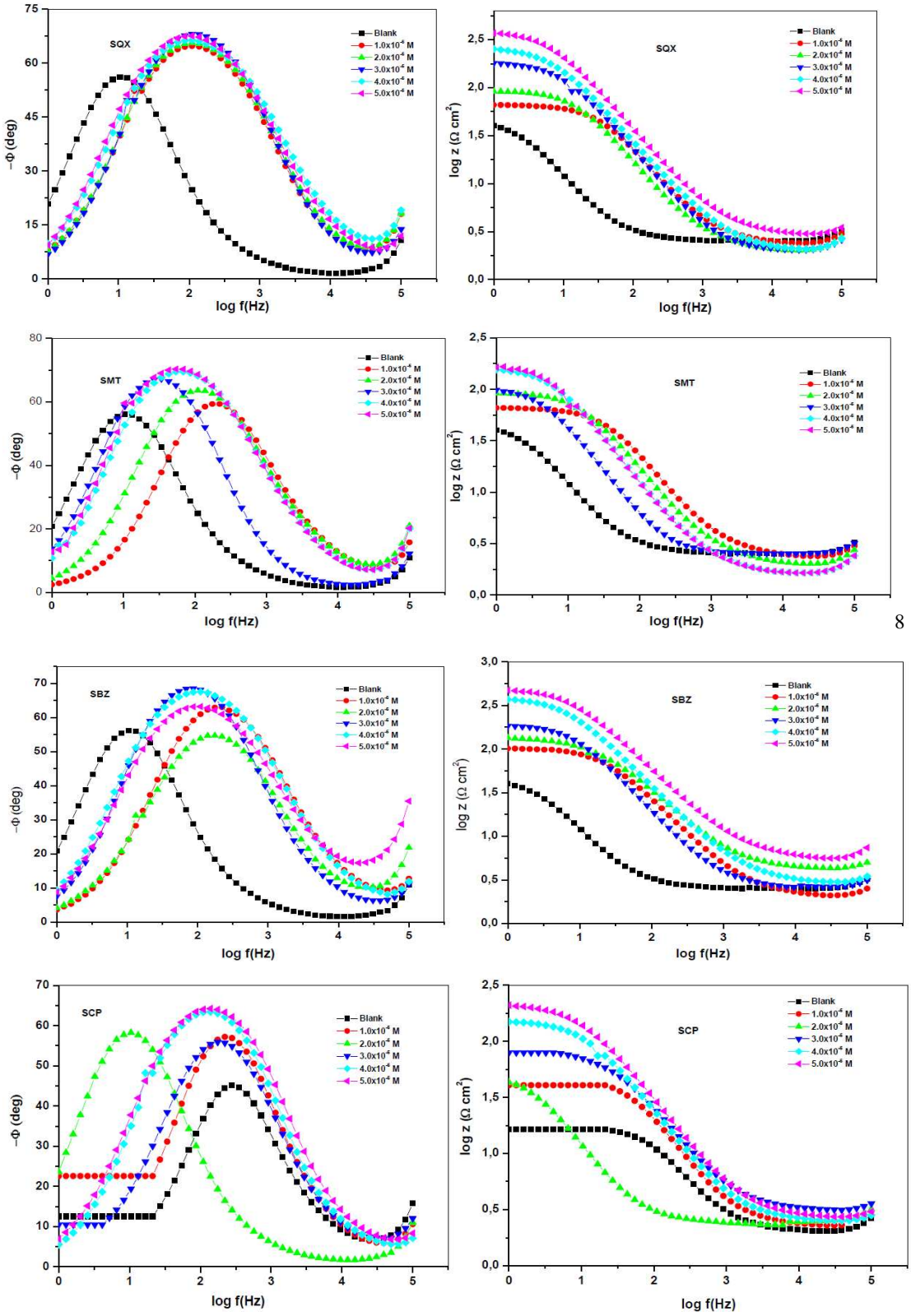

Figure 4. Bode plots of mild steel in 1 M HCl in the absence and presence of different concentrations of of inhibitor compounds.

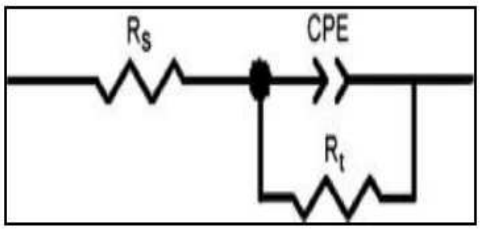

Figure 5. Equivalent circuit used to fit the impedance spectra obtained for mild steel corrosion in 1.0 M HCl in the absence and presence of SQX, SMT, SBZ and SCP.

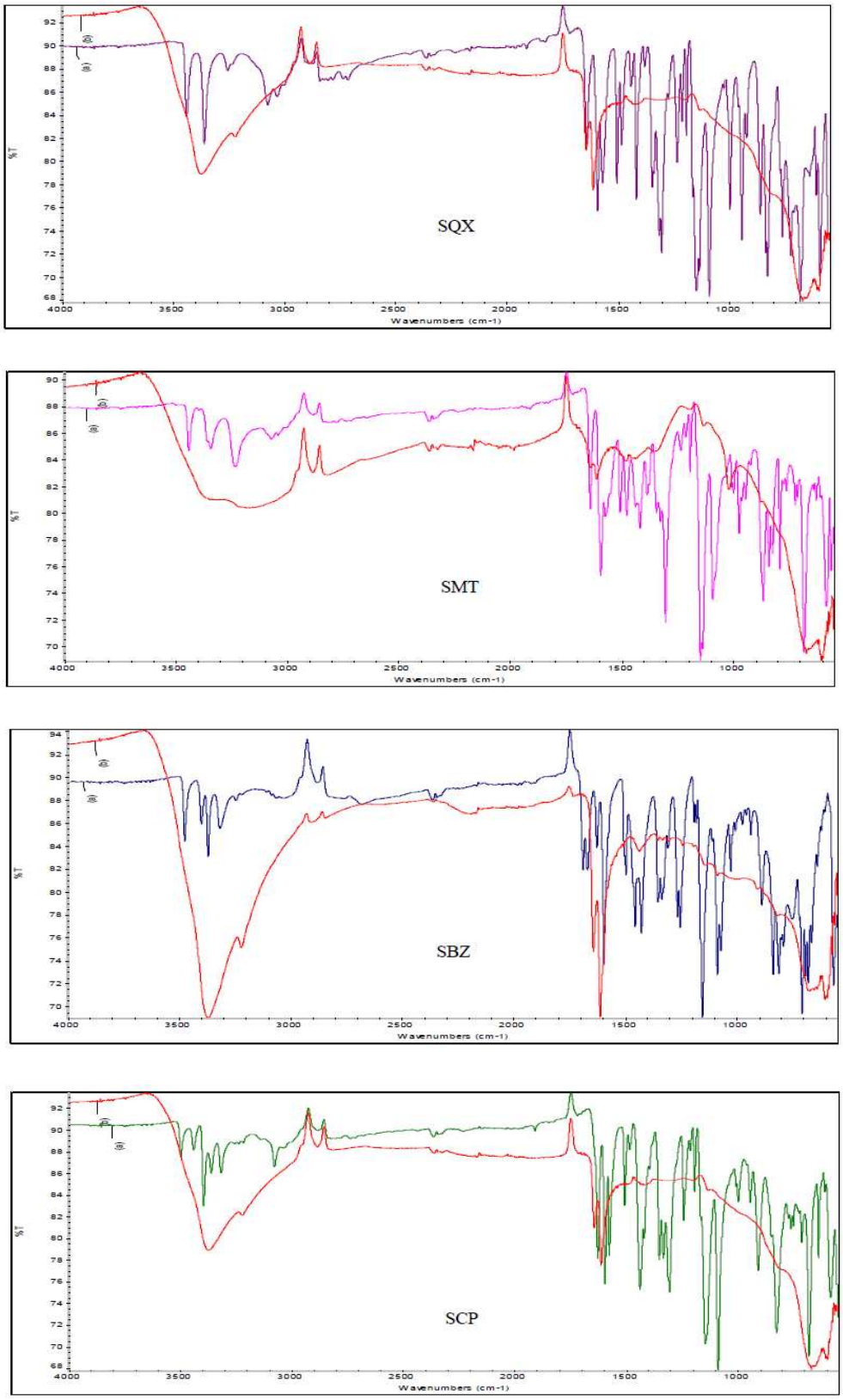

Figure 6. FT-IR spectra: (a) studied corrosion inhibitors and (b) adsorption films formed on the mild steel in 1.0 M HCl using different corrosion inhibitors.

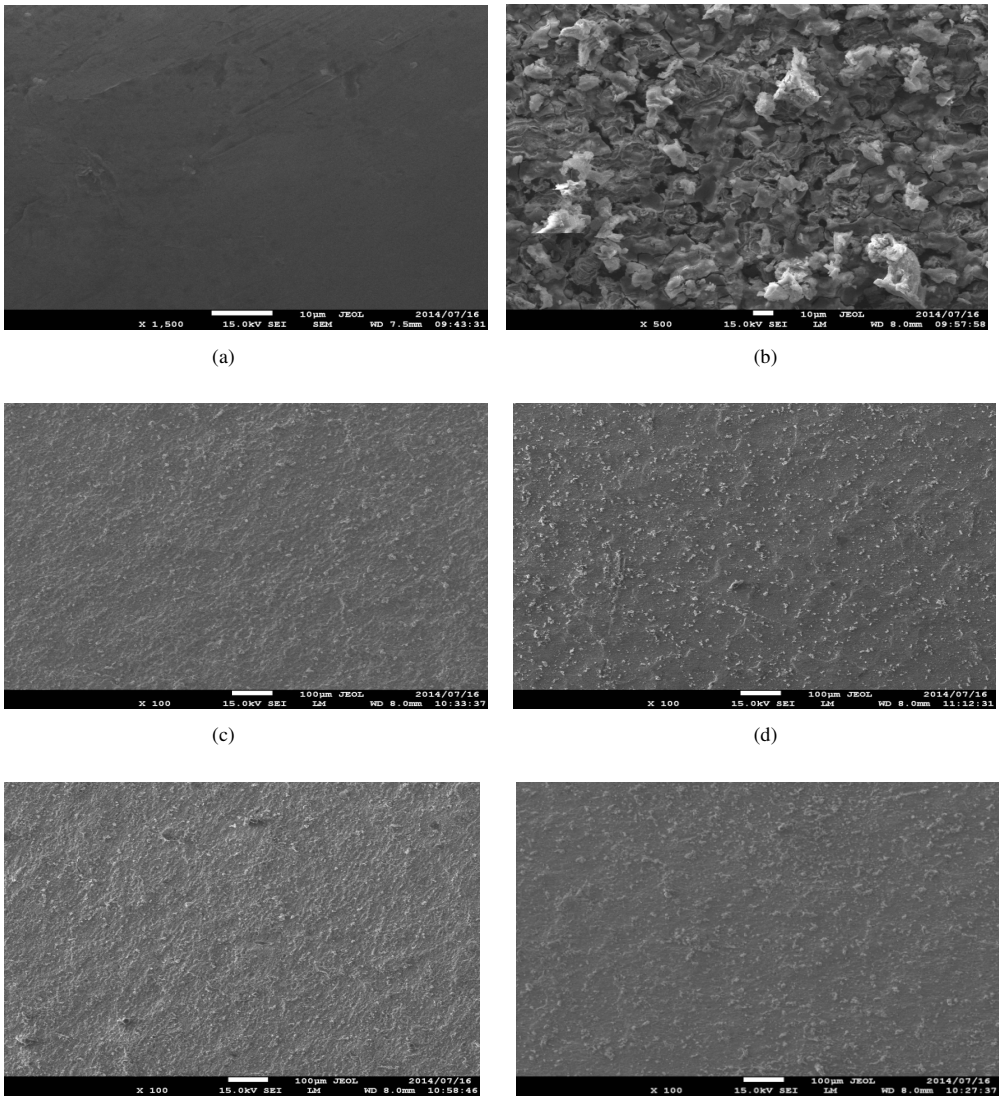

Figure 7. SEM micrographs of the surface of mild steel: (a) plain mild steel (b) mild steel immersed in HCl uninhibited and mild steel immersed in HCl in the presence of (c) SBZ (d) SCP (e) SMT (f) SQX

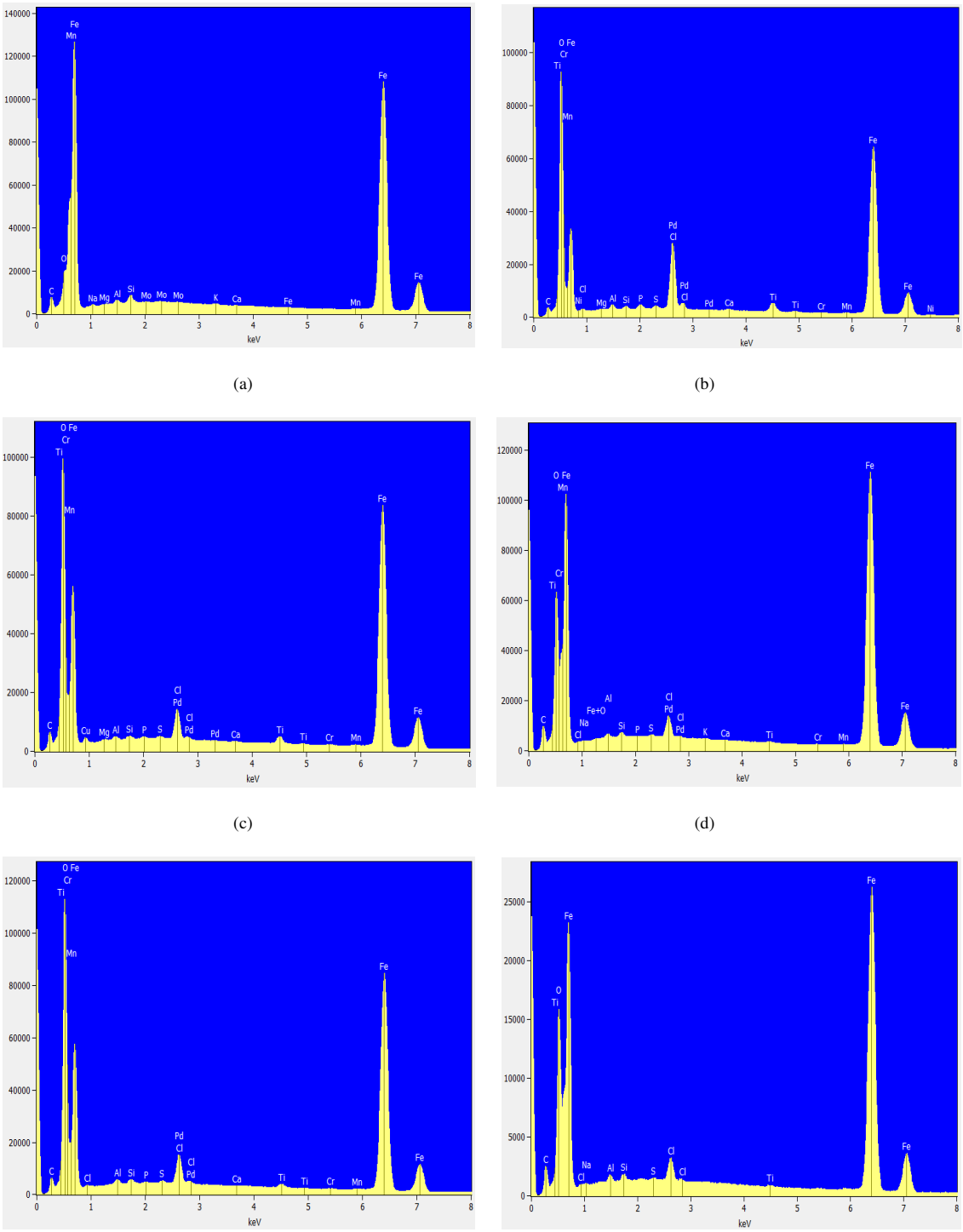

Figure 8. EDS spectra of mild steel (a) plain mild steel (b) mild steel immersed in HCl uninhibited and mild steel immersed in HCl in the presence of (c) SBZ (d) SCP (e) SMT (f) SQX

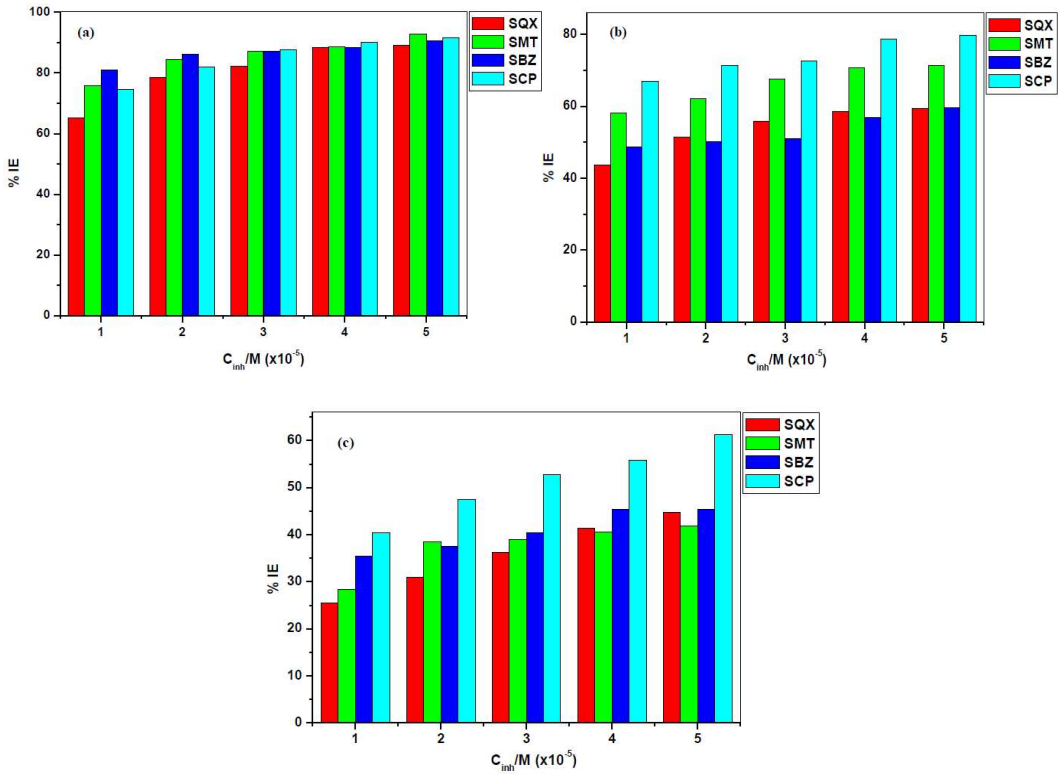

Figure 9. Variations of the percentage inhibition efficiencies with various concentrations of the utilized corrosion inhibitors at (a) 30 °C, (b) 40 °C and (c) 50 °C.

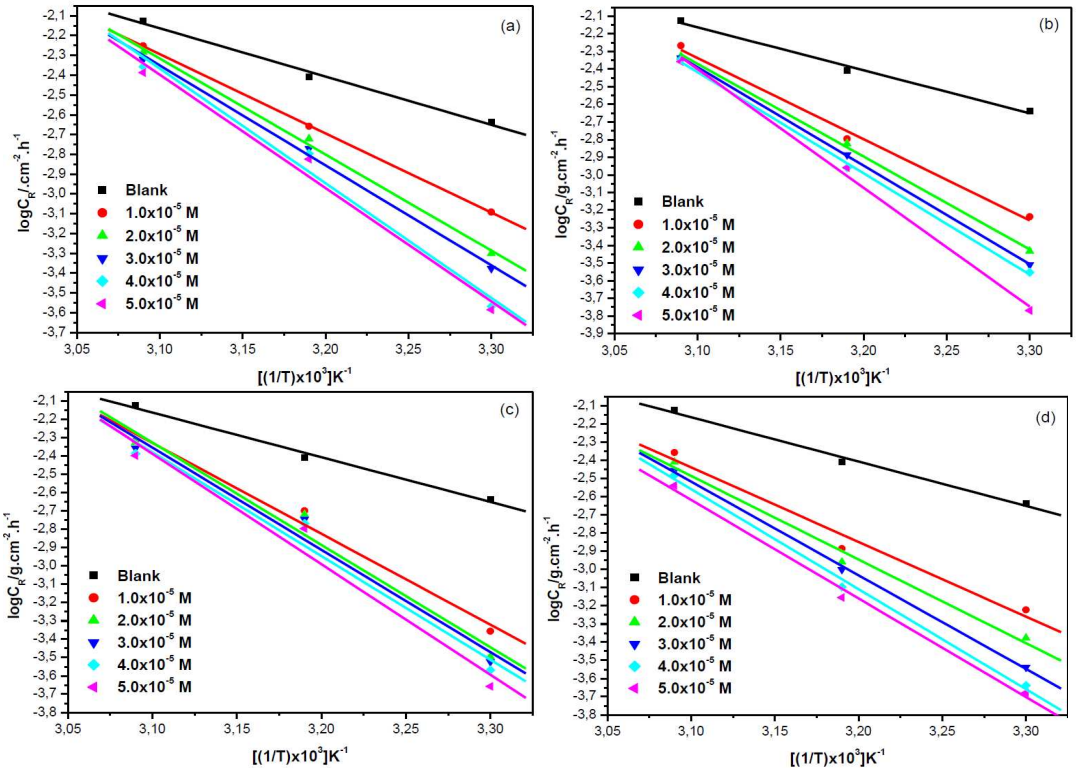

Figure 10. Arrhenius plots for the corrosion of mild steel in 1.0 M HCl in the absence and presence of various concentrations of the utilized corrosion inhibitors: (a) SQX, (b) SMT, (c) SBZ and (d) SCP.

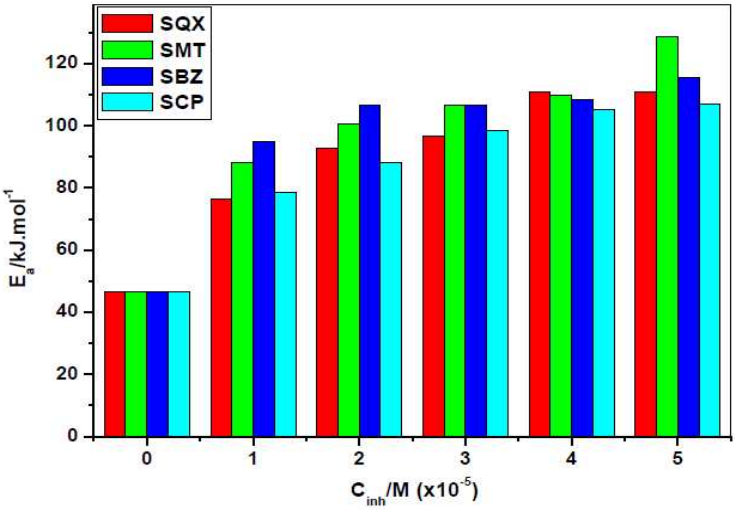

Figure 11. Variation of the activation energy with the concentration of the utilized corrosion inhibitors:

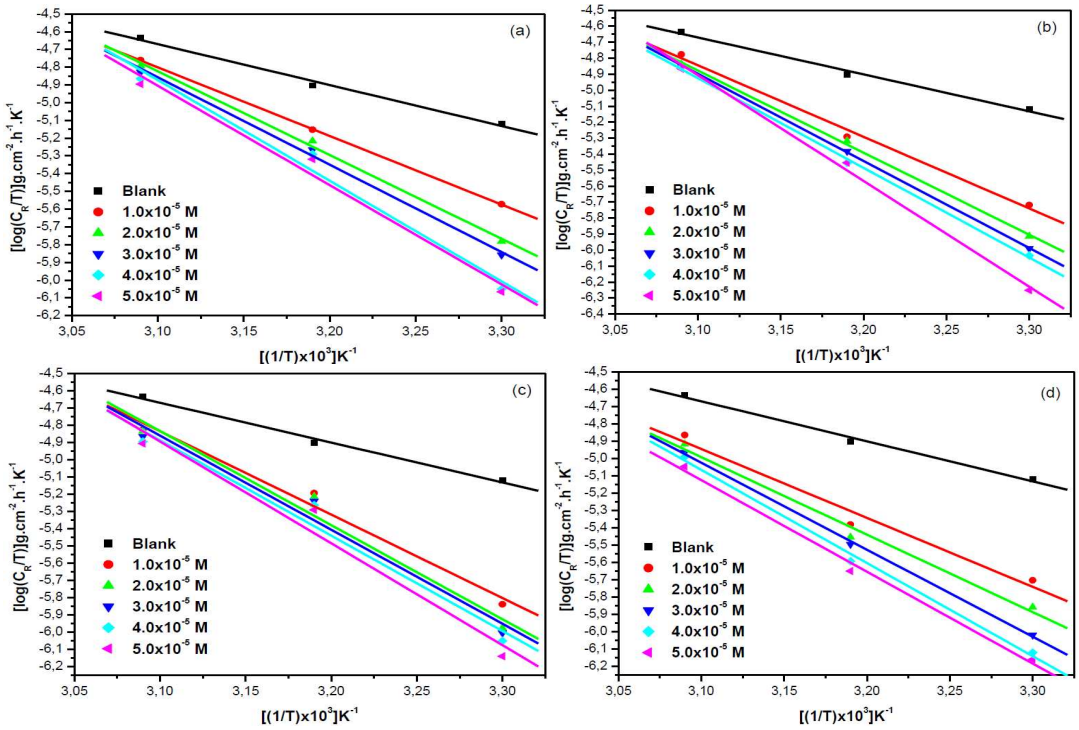

Figure 12. Transition state plots for the corrosion of mild steel in 1.0 M HCl in the absence and presence of various concentrations of the utilized corrosion inhibitors: (a) SQX, (b) SMT, (c) SBZ and (d) SCP.

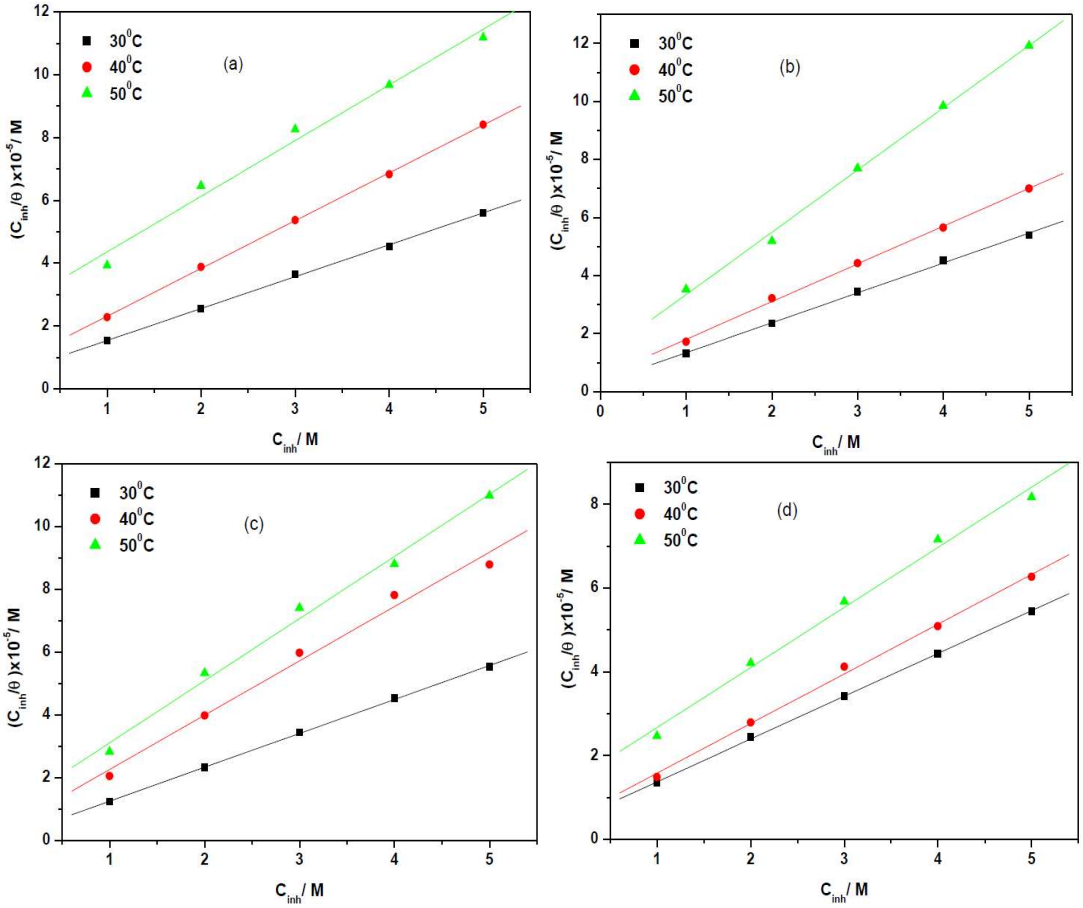

Figure 13. Langmuir adsorption isotherms for the corrosion of mild steel in 1.0 M HCl at various temperatures for the utilized corrosion inhibitors: (a) SQX, (b) SMT, (c) SBZ and (d) SCP (from the weight loss method).

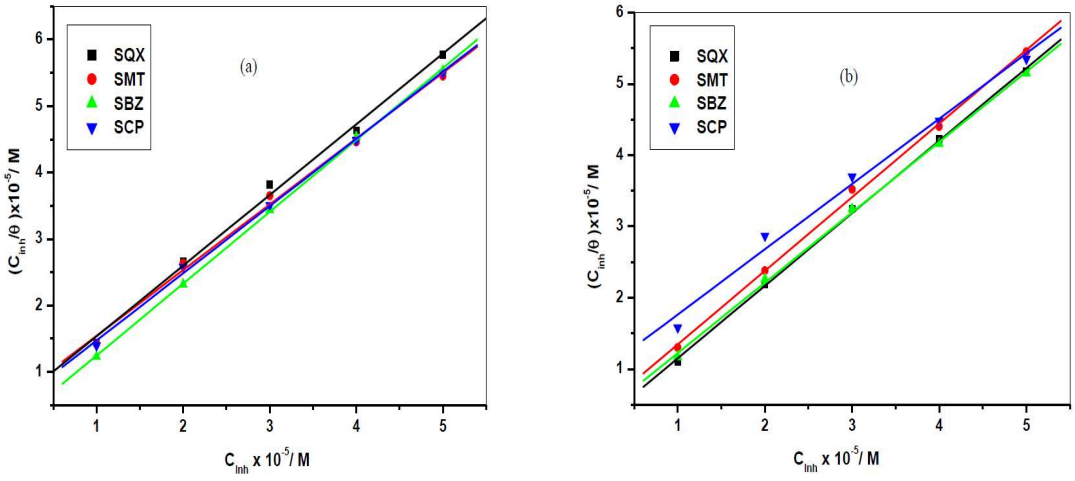

Figure 14. Langmuir adsorption isotherms obtained using the (a) PDP and (b) EIS data for the corrosion of mild steel in 1.0 M HCl for the utilized corrosion inhibitors at 30 °C.

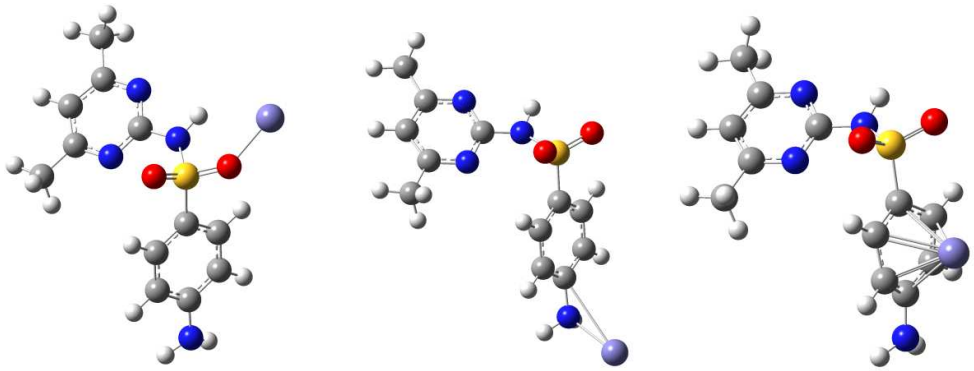

22.254 6.046 2.465

Figure 15. The optimized Fe···SMT complexes, G96lyp/6-31+G(d) results *in vacuo*. The binding energy value (kcal/mol) is reported below each complex.

Table 1 Potentiodynamic polarization (PDP) parameters such as corrosion potential (E_{corr}), corrosion current density (i_{corr}) and anodic and cathodicTafel slopes (b_a and b_c) using different inhibitors

Inhibitor	Inhibitor Conc. (M)	$-E_{corr}$(mV)/SCE with Ag/AgCl	i_{corr}(mA.cm^{-2})	R_p(10^{-1}) (Ohm)	b_a (mV.dec^{-1})	b_c (mV.dec^{-1})	%IE$_{PDP}$	%IE$_{WL}$
Blank		513	3.63	1.62	66	75	-	-
	1.0×10^{-5}	495	1.11	6.56	31	54	69.42	65.32
	2.0×10^{-5}	481	0.91	5.17	36	69	74.93	78.62
SQX	3.0×10^{-5}	482	0.77	6.04	19	58	78.62	82.19
	4.0×10^{-5}	487	0.49	3.80	37	34	86.39	88.36
	5.0×10^{-5}	503	0.48	5.71	26	25	86.72	89.07
	1.0×10^{-5}	501	1.08	6.04	40	47	70.25	75.75
	2.0×10^{-5}	499	0.86	4.21	44	41	76.22	84.49
SMT	3.0×10^{-5}	499	0.65	5.93	50	45	82.23	87.20
	4.0×10^{-5}	506	0.38	2.12	17	14	89.64	88.55
	5.0×10^{-5}	502	0.30	1.08	04	17	91.71	92.77
	1.0×10^{-5}	505	0.88	3.18	21	44	80.99	75.81
	2.0×10^{-5}	502	0.64	7.25	24	50	86.22	82.34
SBZ	3.0×10^{-5}	503	0.37	3.90	14	17	87.17	89.86
	4.0×10^{-5}	503	0.35	3.87	16	15	88.36	90.24
	5.0×10^{-5}	507	0.29	1.27	02	20	90.49	92.06
	1.0×10^{-5}	501	1.03	8.12	33	42	71.63	74.55
	2.0×10^{-5}	504	0.81	8.12	35	40	77.60	82.08
SCP	3.0×10^{-5}	506	0.53	3.33	21	15	85.51	87.65
	4.0×10^{-5}	504	0.39	2.67	15	16	89.09	90.21
	5.0×10^{-5}	505	0.33	3.20	15	16	90.88	91.72

Table 2 Electrochemical impedance (EIS) parameters such as the resistance of charge transfer (R_t), constant phase element (CPE) and the CPE exponent (n) using different inhibitors.

Inhibitor	Inhibitor Conc. (M)	R_s (Ω cm^2)	R_t (Ω cm^2)	n	CPE (μF cm^{-2})	%IE$_{EIS}$	%IE$_{WL}$
Blank		2.05	15.00	0.87	265.1	-	-
	1.0×10^{-5}	1.97	162.6	0.85	205.7	90.77	65.32
	2.0×10^{-5}	1.96	176.1	0.83	187.6	91.48	78.62
SQX	3.0×10^{-5}	1.98	196.1	0.83	166.8	92.38	82.19
	4.0×10^{-5}	1.99	287.6	0.80	136.5	94.78	88.36
	5.0×10^{-5}	2.76	466.0	0.76	99.3	96.78	89.07
	1.0×10^{-5}	2.42	64.7	0.87	145.8	76.81	75.75
	2.0×10^{-5}	2.06	94.1	0.86	136.8	84.05	84.49
SMT	3.0×10^{-5}	2.57	101.8	0.93	134.7	85.25	87.20
	4.0×10^{-5}	1.70	166.5	0.88	111.2	90.99	88.55
	5.0×10^{-5}	1.69	181.4	0.88	107.8	91.73	92.77
	1.0×10^{-5}	2.09	103.8	0.85	146.2	85.54	75.81
	2.0×10^{-5}	4.19	132.5	0.80	134.6	88.67	82.34
SBZ	3.0×10^{-5}	2.65	192.5	0.89	136.5	92.20	89.86
	4.0×10^{-5}	2.99	401.0	0.84	112.4	96.25	90.24
	5.0×10^{-5}	5.35	529.0	0.79	94.6	97.16	92.06
	1.0×10^{-5}	2.36	40.7	0.88	159.4	63.14	74.55
	2.0×10^{-5}	2.47	49.3	0.90	144.0	69.57	82.08
SCP	3.0×10^{-5}	3.30	79.3	0.85	147.6	81.08	87.65
	4.0×10^{-5}	2.65	140.0	0.92	106.4	89.28	90.21
	5.0×10^{-5}	2.59	232.5	0.79	105.7	93.54	91.72

Table 3 Peaks and their identification, from FT-IR spectra of the studied corrosion inhibitors and adsorption films formed (SQX-MX, SMT-MS, SBZ-MS and SCP-MS) on the mild steel in 1.0 M HCl using different corrosion inhibitors.

Functional Groups	**Peaks from FT-IR Spectra (cm^{-1})**							
	SQX	SQX-MS	SMT	SMT-MS	SBZ	SBZ-MS	SCP	SCP-MS
N-H	3356.94	3371.95	3342.84	-	3365.41	3366.31	3399.99	3393.62
NH_2	1590.11	1638.98	1570.68	1641.80	1592.88	1639.77	1624.57	1622.06
C=C	1502.34	1607.95	1591.80	1605.13	1452.55	1609.25	1593.11	1596.67
O=S=O	1343.94	-	1300.96	-	1331.61	-	1330.51	-
C-N	1146.34	1136.85	1143.93	1134.03	1151.12	1139.67	1141.92	1137.30
γ-Fe_2O_3	-	667.21	-	667.60	-	667.05	-	667.25

Table 4 Percentage inhibition efficiencies and corrosion rates values obtained from the weight loss of mild steel in 1.0 M HCl in the absence and presence of various concentrations of inhibitors.

Inhibitor	Inhibitor Conc. (M)	Temperature					
		30 °C		40 °C		50 °C	
		$\%IE_{WL}$	$C_R(g.cm^{-2}.h^{-1})$	$\%IE_{WL}$	$C_R(g.cm^{-2}.h^{-1})$	$\%IE_{WL}$	$C_R(g.cm^{-2}.h^{-1})$
Blank	0.0	-	0.0023	-	0.0039	-	0.0075
	1.0×10^{-5}	65.32	0.00081	43.84	0.0022	25.44	0.0056
	2.0×10^{-5}	78.62	0.00050	51.43	0.0019	30.95	0.0052
SQX	3.0×10^{-5}	82.19	0.00042	55.87	0.0017	36.31	0.0048
	4.0×10^{-5}	88.36	0.00027	58.59	0.0016	41.36	0.0044
	5.0×10^{-5}	89.07	0.00026	59.43	0.0015	44.72	0.0041
	1.0×10^{-5}	75.75	0.00058	58.07	0.0016	28.34	0.0054
	2.0×10^{-5}	84.49	0.00037	62.10	0.0015	38.47	0.0047
SMT	3.0×10^{-5}	87.20	0.00031	67.73	0.0013	38.95	0.0046
	4.0×10^{-5}	88.55	0.00028	70.73	0.0011	40.59	0.0045
	5.0×10^{-5}	92.77	0.00017	71.38	0.0011	41.93	0.0044
	1.0×10^{-5}	80.99	0.00044	48.71	0.0020	35.50	0.0048
	2.0×10^{-5}	86.22	0.00032	50.14	0.0019	37.50	0.0047
SBZ	3.0×10^{-5}	87.17	0.00030	51.15	0.0018	40.48	0.0044
	4.0×10^{-5}	88.36	0.00027	56.88	0.0017	45.38	0.0041
	5.0×10^{-5}	90.49	0.00022	59.60	0.0016	45.46	0.0040
	1.0×10^{-5}	74.55	0.00060	67.05	0.0013	40.48	0.0044
	2.0×10^{-5}	82.08	0.00042	71.49	0.0011	47.54	0.0039
SCP	3.0×10^{-5}	87.65	0.00029	72.78	0.0010	52.82	0.0035
	4.0×10^{-5}	90.21	0.00023	78.65	0.0008	55.87	0.0033
	5.0×10^{-5}	91.72	0.00021	79.79	0.0007	61.23	0.0029

Table 5 Kinetic and activation parameters (derived from the Arrhenius and transition-states plots) for mild steel in 1.0 M HCl in the absence and presence of various concentrations of inhibitors.

Inhibitor	Inhibitor Conc. (M)	Activation Energy (E_a/kJ.mol^{-1})	Enthalpy of Activation (ΔH^*/ kJ.mol^{-1})	Entropy of Activation (ΔS^*/ J.mol^{-1}.K^{-1})
Blank	0.0	46.64	44.09	–150.29
	1.0×10^{-5}	76.54	73.90	–60.36
	2.0×10^{-5}	92.83	90.28	–9.98
SQX	3.0×10^{-5}	96.58	94.12	1.28
	4.0×10^{-5}	110.86	108.40	45.27
	5.0×10^{-5}	111.07	107.02	40.37
	1.0×10^{-5}	88.04	85.60	–24.92
	2.0×10^{-5}	100.67	98.17	13.43
SMT	3.0×10^{-5}	106.80	104.26	31.94
	4.0×10^{-5}	109.86	107.27	40.87
	5.0×10^{-5}	128.81	126.45	100.57
	1.0×10^{-5}	94.94	92.38	–3.71
	2.0×10^{-5}	106.83	104.29	33.24
SBZ	3.0×10^{-5}	106.76	104.27	32.54
	4.0×10^{-5}	108.25	105.66	36.47
	5.0×10^{-5}	115.42	112.87	58.65
	1.0×10^{-5}	78.50	76.00	–56.63
	2.0×10^{-5}	87.97	85.43	–28.27
SCP	3.0×10^{-5}	98.53	95.97	3.81
	4.0×10^{-5}	105.26	102.72	23.94
	5.0×10^{-5}	107.03	101.15	17.95

Table 6 Thermodynamic and adsorption parameters (derived from the Langmuir adsorption isotherms) for mild steel in 1.0 M HCl at various temperatures for the utilized corrosion inhibitors using weight loss method

Inhibitor	Temperature (°C)	r^2	Slope	K_{ads} (M^{-1})	ΔG^0_{ads} ($kJ.mol^{-1}$)	ΔH^0_{ads} ($kJ.mol^{-1}$)	ΔS^0_{ads} ($J.mol^{-1}.K^{-1}$)
	30	0.999	1.015	1.898	−11.73		
SQX	40	0.999	1.152	1.264	−11.06	−65.12	−175
	50	0.992	1.771	0.387	−8.23		
	30	0.999	1.030	3.164	−13.02		
SMT	40	0.999	1.299	1.972	−12.22	−55.64	−140
	50	0.998	2.144	0.829	−10.28		
	30	0.999	1.081	5.988	−14.63		
SBZ	40	0.993	1.732	1.893	−12.11	−77.51	−208
	50	0.996	1.126	0.888	−10.47		
	30	0.999	1.021	2.833	−12.74		
SCP	40	0.998	1.186	2.538	−12.87	−51.38	−126
	50	0.996	1.435	0.811	−10.22		

Table 7 Thermodynamic and adsorption parameters (derived from the Langmuir adsorption isotherms) for mild steel in 1.0 M HCl at 30 °C using PDP and EIS for the utilized corrosion inhibitors.

Inhibitor	Method	r^2	Slope	K_{ads} (M^{-1})	ΔG^0_{ads} ($kJ.mol^{-1}$)
	PDP	0.997	1.063	2.105	-11.99
SQX	EIS	0.999	1.017	7.410	-15.16
	PDP	0.997	0.989	1.801	-11.60
SMT	EIS	0.999	1.032	3.184	-13.04
	PDP	0.999	1.081	5.988	-14.63
SBZ	EIS	0.999	0.986	4.170	-13.72
	PDP	0.999	1.011	2.159	-12.06
SCP	EIS	0.995	0.918	1.180	-10.54

Table 8 Quantum chemical parameters for the investigated compounds

Quantum chemical parameter	**Structures**			
	SMT	SCP	SBZ	SQX
E_{HOMO} (eV)	-6.228	-6.574	-6.536	-6.442
E_{LUMO} (eV)	-1.273	-2.156	-1.820	-2.136
ΔE (eV)	4.955	4.418	4.716	4.306
μ (Debye)	7.589	6.271	7.160	6.649